JACS
JOURNAL OF THE AMERICAN CHEMICAL SOCIETY
Article
pubs.acs.org/JACS

# Alkylated Selenophene-Based Ladder-Type Monomers via a Facile Route for High-Performance Thin-Film Transistor Applications

Zhuping Fei,[†,§] Yang Han,[*,†,‡,§] Eliot Gann,[∥] Thomas Hodsden,[†,§] Anthony S. R. Chesman,[⊥] Christopher R. McNeill,[∥] Thomas D Anthopoulos,[‡,§,#] and Martin Heeney[*,†,§]

[†]Department of Chemistry, [‡]Department of Physics, and [§]Centre for Plastic Electronics, Imperial College London, Exhibition Road, London SW7 2AZ, United Kingdom

[∥]Department of Materials Science and Engineering, Monash University, Clayton, Victoria 3800, Australia

[⊥]CSIRO Manufacturing, Ian Wark Laboratories, Clayton, Victoria 3168, Australia

[#]Division of Physical Sciences and Engineering, King Abdullah University of Science and Technology, Thuwal 23955-6900, Saudi Arabia

Supporting Information

**ABSTRACT:** We report the synthesis of two new selenophene-containing ladder-type monomers, cyclopentadiselenophene (CPDS) and indacenodiselenophene (IDSe), via a 2-fold and 4-fold Pd-catalyzed coupling with a 1,1-diborylmethane derivative. Copolymers with benzothiadiazole were prepared in high yield by Suzuki polymerization to afford materials which exhibited excellent solubility in a range of nonchlorinated solvents. The CPDS copolymer exhibited a band gap of just 1.18 eV, which is among the lowest reported for donor−acceptor polymers. Thin-film transistors were fabricated using environmentally benign, nonchlorinated solvents, with the CPDS and IDSe copolymers exhibiting hole mobility up to 0.15 and 6.4 $cm^2\ V^{-1}\ s^{-1}$, respectively. This high performance was achieved without the undesirable peak in mobility often observed at low gate voltages due to parasitic contact resistance.

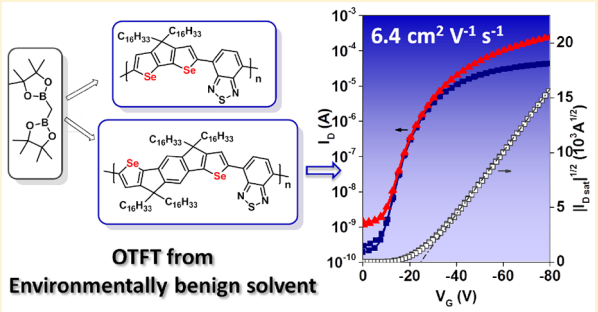


## INTRODUCTION

The past three decades has seen tremendous effort devoted to the development of conjugated small molecules and polymers for low-cost, flexible, and large-area electronics.[1,2] A variety of building blocks have been developed and incorporated into conjugated architectures for high-performance organic thin-film transistor (OTFTs) and organic photovoltaic (OPV) applications.[3−6] Among these building blocks, ladder-type fused aromatic monomers have attracted much interest because of their unique structures and intriguing electrical properties. Covalently flanked adjacent aromatic units force the ladder-type monomer to adopt a nearly coplanar rigid conformation.[7,8] The use of this kind of coplanar building block can potentially elongate the effective conjugation length, facilitating $\pi$-electron delocalization and decreasing the reorganizational energy, thus enhancing the intrinsic charge carrier mobility.[9−11] Many of the high-performance ladder-type monomers reported to date are thiophene-based, in which the thiophene units have been bridged by a variety of heteroatoms. In addition to their electronic effects, these bridging atoms are typically utilized to incorporate solubilizing groups to enable processability. For example, many polymers and small molecules based on cyclopentadithiophene (CDT) and indacenodithiophene (IDT) with carbon as the bridging atom exhibit promising performance in solution-processed high-performance OTFTs[12−16] and OPVs.[3] Different strategies have been employed to modify the structure of the ladder-type units to adjust the electronic energy levels and aggregation state of the resulting semiconductor, for example, replacing the bridging carbon with a Si or Ge atom, or further extending the conjugation length by flanking with fused aromatic rings.[7]

Replacing the sulfur atom in the thiophene ring is another approach to control the properties of semiconducting molecules. The larger size of Se over S reduces overlap with the adjacent $\pi$-system, and the resulting reduction in aromaticity of selenophene compared to thiophene increases the quinoidal character of the polymer backbone, which usually results in a reduced band gap.[17,18] The more polarizable Se can also enhance intermolecular interactions of conjugated backbones in some cases, and many different selenophene-containing conjugated polymers have been reported to give improved device performance, especially charge carrier mobility, over their thiophene-containing analogues.[18−34] One consequence of these changes is that selenophene-containing polymers are often poorly soluble, and those that are soluble

Received: March 28, 2017
Published: May 26, 2017




DOI: 10.1021/jacs.7b03099
J. Am. Chem. Soc. 2017, 139, 8552−8561

typically require the use of highly chlorinated, high-boiling-point solvents such as 1,2-dichlorobenzene. However, such solvents are very unattractive for processing due to their detrimental environmental impact and health hazards.[35] In this respect, we were interested to develop new fused ladder-type selenophene monomers, since the bridging position could be utilized to promote solubility in nonchlorinated solvents via the use of very long alkyl side chains. However, until now, there have been few examples of selenophene-based ladder-type building blocks reported, possibly due to the difficulty in the functionalization of selenophene compared to thiophene.[20,36−40] Of the limited selenophene-containing ladder-type building blocks reported, it is noticeable that carbon-bridged examples always incorporate a bridging phenylalkyl or phenylalkoxy group as the solubilizing group. This is likely due to synthetic reasons, since Friedel−Crafts-type ring-closing reactions are utilized from the corresponding (stable) triaryl cations. However, in many cases it is undesirable for device applications to utilize aromatic groups directly on the bridging carbon because of the rather large steric hindrance compared to that of simple linear alkyl groups. This can inhibit close packing of the polymer backbones, resulting in reduced device performance, particularly for transistor applications.

Here we report a facile route for the first reported preparation of the alkylated selenophene-based fused-ring ladder monomers cyclopentadiselenophene (CPDS) and indacenodiselenophene (IDSe). We report their corresponding conjugated polymers PCPDSBT and PIDSeBT, by copolymerization with an electron acceptor unit, 2,1,3-benzothiadiazole (BT). The resulting polymers exhibit excellent solubility in nonchlorinated solvents such as tetralin, and organic thin-film transistors fabricated from these solutions exhibit a saturated mobility up to 6.4 $cm^2\ V^{-1}\ s^{-1}$. This is among the highest hole mobility values reported for devices fabricated from nonchlorinated solvents.[35] Importantly, all optimized devices show clean transistor behavior without the fluctuations in the derived carrier mobility at low gate voltages that are apparent in numerous previous reports of high-mobility polymers.[41,42]

## EXPERIMENTAL SECTION

**General Procedures.** All reactions were carried out in oven-dried glassware under Ar using solvents and reagents as commercially supplied, unless otherwise stated. 2,1,3-Benzothiadiazole-4,7-bis(boronic acid pinacol ester) (**6**) was purified by recrystallization from hexane before use. (3,3′-Dibromo-[2,2′-biselenophene]-5,5′-diyl)bis(trimethylsilane) (**1**),[43] bis(4,4,5,5-tetramethyl-1,3,2-dioxaborolan-2-yl)methane,[44] 2,5-dibromoselenophene (**7**),[45] and 1,4-dibromo-2,5-diiodobenzene (**10**)[46] were synthesized by the reported methods. $^1$H and $^{13}$C NMR spectra were recorded on a Bruker AV-400 (400 MHz), using the residual solvent resonance of $CDCl_3$ or $d_2$-1,1,2,2-tetrachloroethane, and the chemical shifts are given in parts per million. Elemental analysis was performed in a Thermo Scientific (Calro Erba) elemental analyzer, configured for the percentage of C, H, and N. Number-average ($M_n$) and weight-average ($M_w$) molar masses were determined by an Agilent Technologies 1200 series gel permeation chromatography (GPC) instrument running in chlorobenzene at 80 °C, using two PL mixed B columns in series, and calibrated against narrow polydispersity polystyrene standards. Matrix-assisted laser desorption/ionization time-of-flight (MALDI-TOF) mass spectrometry was performed on a Bruker ultrafleXtreme MALDI-TOF analyzer. Anthracene (or 2,5-dihydroxybenzoic acid) and myoglobin were used as the matrix and calibration internal standard, respectively. Thermogravimetric analysis (TGA) was carried out using a PerkinElmer Pyris 1 TGA machine, with heating from 50 to 700 °C at a heating rate of 20 °C/min under $N_2$. Differential scanning calorimetry (DSC) was performed on a TA Instruments Discovery differential calorimeter at a scan rate of 10 °C/min from 0 to 300 °C under $N_2$. UV−vis spectra were recorded on a UV-1601 Shimadzu UV−vis spectrometer. Photoelectron spectroscopy in air (PESA) measurements were recorded with a Riken Keiki AC-2 PESA spectrometer with a power setting of 10 nW and a power number of 0.5. Samples for PESA were prepared on glass substrates by spin-coating. Atomic force microscopy (AFM) images were obtained with a Picoscan PicoSPM LE scanning probe in tapping mode. Samples were prepared following the same procedures for fabrication of transistors, except that the Au contacts, CYTOP dielectric, and Al gate were not applied. Density functional theory (DFT) calculations were modeled using Gaussian at the B3LYP/6-31G* level. The side chains were modified to ethyl groups to simplify the calculations.

**OTFT (Organic Thin-Film Transistor) Device Fabrication.** A solution of polymer was prepared by dissolving the polymer in tetralin at a concentration of 10 mg/mL. Transistors were prepared by first thermally evaporating Au (40 nm) onto glass substrates through a shadow mask to form bottom-source/drain (S/D) electrodes, which were then treated with a self-assembled monolayer (SAM) of pentafluorobenzenethiol (PFBT) to improve the work function. The SAM treatment step was carried out by immersing the substrates with patterned Au electrodes in a solution containing a 1:1000 ratio of PFBT in ethanol for 30 min before rinsing them off with plenty of ethanol to remove the excess materials and annealing at 100 °C for 15 min. Polymer was then spin coated at 1000 rpm for 60 s on top of the substrates with PFBT-treated bottom electrodes. The obtained films were then thermally annealed at 200 or 270 °C for 30 min under nitrogen. A 900 nm layer of CYTOP (Asahi Glass, type CTL-809M) dielectric was then deposited on top of the polymer layer by spin coating at 2000 rpm for 60 s followed by an annealing step at 100 °C for 30 min. The transistor structure was then completed by thermally evaporating 50 nm of Al gate electrodes through a shadow mask, resulting in the bottom-contact, top-gate architecture. The channel width and length of the final transistors were 1000 $\mu$m and 30 or 40 $\mu$m, respectively. Transistor characterization was carried out under nitrogen using a Keithley 4200 parameter analyzer. Linear mobility was calculated according to the following equation:

$$\mu_{lin} = \frac{L}{WC_iV_D}\left(\frac{\partial I_{D,lin}}{\partial V_G}\right)$$

The saturation mobility was extracted from the slope of $I_D^{1/2}$ vs $V_G$:

$$\mu_{sat} = \frac{2L}{WC_i}\left(\frac{\partial \sqrt{I_{D,sat}}}{\partial V_G}\right)^2$$

Copper(I) thiocyante (CuSCN) was dissolved in diethyl sulfide at a concentration of 5 mg/mL and spin cast onto the substrates with prepatterned Au electrodes at 5000 rpm for 30 s. The resulting CuSCN thin film was annealed at 100 °C for 30 min under nitrogen. The polymer solution was then spin cast and annealed following the same procedures as for PFBT devices.

The deep trap densities ($N_{tr}$) of OTFTs were determined from the subthreshold swing ($S$) according to the following equation:[47,48]

$$N_{tr} = \frac{C_i}{e^2}\left(\frac{eS}{kT\ \ln(10)} - 1\right)$$

where $e$ is the elementary charge, $C_i$ the geometric capacitance of the gate dielectric, $V_{on}$ the onset voltage, $k$ the Boltzmann constant, and $T$ the measuring temperature.

The dielectric constant ($\varepsilon$) of CYTOP was determined with capacitance−frequency ($C$−$F$) measurements performed on a parallel plate capacitor structure using an impedance analyzer (Solartron1260). The data yielded a value for the dielectric constant of 2.14, which is in good agreement with the manufacturer's specification (2.0−2.1). The $C_i$ of CYTOP was then determined to be 2.10 ± 0.09 nF $cm^{-2}$, according to the following equation:


DOI: 10.1021/jacs.7b03099
J. Am. Chem. Soc. 2017, 139, 8552−8561

$$C_i = \frac{\varepsilon\varepsilon_0}{d}$$

where $\varepsilon$ is the dielectric constant of CYTOP ($\varepsilon$ = 2.14), $\varepsilon_0$ the vacuum permittivity, and $d$ the thickness of the CYTOP dielectric layer (~900 nm).

**Grazing-Incidence Wide-Angle X-ray Scattering (GIWAXS).** GIWAXS measurements were performed at the small-angle X-ray scattering/wide-angle X-ray scattering (SAXS/WAXS) beamline at the Australian Synchrotron.[49] Two-dimensional scattering patterns were recorded on a Dectris Pilatus 1M detector with 11 keV photons used to probe the samples. An angle of incidence close to the critical angle (~0.13°) was used. The total exposure time was 3 s, with the reported images a composite of three separate 1 s exposures taken with different lateral detector offsets to fill in the regions missed by gaps in the detector. A silver behenate standard was used to calibrate the sample-to-detector distance. The results were analyzed using NIKA 2D[50] implemented in IgorPro.

**Synthesis.** *4H-Cyclopenta[2,1-b:3,4-b′]diselenophene (**2**).* (3,3′-Dibromo-[2,2′-biselenophene]-5,5′-diyl)bis(trimethylsilane) (4.3 g, 7.6 mmol), bis(4,4,5,5-tetramethyl-1,3,2-dioxaborolan-2-yl)methane (3.07 g, 11.5 mmol), and bis(tri-*tert*-butylphosphine)palladium (0.39 g, 0.76 mmol) were added into a 100 mL two-neck round-bottom flask under argon. Then predegassed dioxane (40 mL) and 8 M KOH (1.44 mL, 11.5 mmol) were added. The mixture was thoroughly degassed under argon and stirred for 24 h at 30 °C. Additional KOH (2.88 mL, 23.0 mmol) was added to the mixture, and the reaction was heated for 24 h at 60 °C. Water (30 mL) was added and the mixture extracted (3 × 50 mL of dichloromethane (DCM)). The combined organics were dried by $MgSO_4$, filtered, and concentrated under reduced pressure. The residue was purified by silica gel chromatography (eluent hexane) to afford a pale yellow solid (1.21 g). To the resulting solid in THF (30 mL) was added tetrabutylammonium fluoride (TBAF) (5.7 mL of a 1 M solution in THF, 5.7 mmol) dropwise at 0 °C. After being stirred at this temperature for 5 min, the mixture was passed through a silica gel plug (5 cm × 5 cm) (eluent hexane). The solvent was removed under reduced pressure, and the residue was purified by silica gel chromatography (eluent hexane) to afford a pale yellow solid (0.77 g, yield 37%). $^1$H NMR ($CDCl_3$, 400 MHz): $\delta$ (ppm) 7.85 (d, $J$ = 5.3 Hz, 2H), 7.34 (d, $J$ = 5.3 Hz, 2H), 3.47 (s, 2H). $^{13}$C NMR ($CDCl_3$, 100 MHz): $\delta$ (ppm) 150.8, 143.6, 129.3, 125.3, 34.6. HRMS (EI$^+$): calcd for $C_9H_6Se_2$, 273.8800; found, 273.8812.

*4,4-Dihexadecyl-4H-cyclopenta[2,1-b:3,4-b′]diselenophene (**3**).* 4*H*-Cyclopenta[2,1-*b*:3,4-*b*′]diselenophene (0.33 g, 1.2 mmol), 1-bromohexadecane (0.81 g, 2.7 mmol), and KI (25 mg, 0.15 mmol) were added into a 50 mL two-neck round-bottom flask under argon, and then degassed DMSO (15 mL) and freshly ground KOH (0.4 g, 7.1 mmol) were added. The mixture was stirred overnight at room temperature. Water (40 mL) was added and the mixture extracted (3 × 30 mL of hexane). The combined organics were dried by $MgSO_4$, filtered, and concentrated under reduced pressure. The residue was purified by silica gel chromatography (eluent hexane) to afford a pale yellow solid (0.63 g, yield 73%). $^1$H NMR ($CDCl_3$, 400 MHz): $\delta$ (ppm) 7.81 (d, $J$ = 5.3 Hz, 2H), 7.15 (d, $J$ = 5.3 Hz, 2H), 1.92−1.73 (m, 4H), 1.42−1.02 (m, 52H), 0.88−0.82 (m, 10H). $^{13}$C NMR ($CDCl_3$, 100 MHz): $\delta$ (ppm) 159.0, 141.2, 129.4, 123.9, 55.6, 37.7, 32.0, 30.0, 29.7−29.6 (overlapping C), 29.4, 24.3, 22.7, 14.1. TOF MS (ES) [M + H]: calcd for $C_{41}H_{71}Se_2$, 723.3881; found, 723.3884.

*2,6-Dibromo-4,4-dihexadecyl-4H-cyclopenta[2,1-b:3,4-b′]diselenophene (**4**).* To a solution of 4,4-dihexadecyl-4*H*-cyclopenta[2,1-*b*:3,4-*b*′]diselenophene (0.63 g, 0.87 mmol) in THF (30 mL) was added *N*-bromosuccinimide (NBS) (0.34 g, 1.9 mmol) in one portion at 0 °C, and the mixture was stirred for 2 h in the absence of light. An aqueous saturated solution of $Na_2SO_3$ (20 mL) was added to quench the reaction. The mixture was extracted with hexane (3 × 30 mL). The combined organics were dried by $MgSO_4$, filtered, and concentrated under reduced pressure. The residue was purified by silica gel chromatography (eluent hexane) to afford a pale yellow solid (0.70 g, yield 91%). $^1$H NMR ($CDCl_3$, 400 MHz): $\delta$ (ppm) 7.11 (s, 2H), 1.78−1.74 (m, 4H), 1.30−1.12 (m, 52H), 0.88−0.82 (m, 10H). $^{13}$C NMR ($CDCl_3$, 100 MHz): $\delta$ (ppm) 156.4, 141.6, 127.1, 114.1, 57.1, 37.6, 31.9, 29.9, 29.7−29.6 (overlapping C), 29.4, 29.3, 24.2, 22.7, 14.1. MALDI-TOF: 878.8 (M$^+$).

*Poly[4,4-Dihexadecyl-4H-cyclopenta[2,1-b:3,4-b′]diselenophene-2,6-diyl-alt-(2,1,3-benzothiadiazole)-4,7-diyl] (PCPDSBT).* A 5 mL high-pressure microwave reactor tube was charged with 2,6-dibromo-4,4-dihexadecyl-4*H*-cyclopenta[2,1-*b*:3,4-*b*′]diselenophene (88.8 mg, 0.1 mmol), 2,1,3-benzothiadiazole-4,7-bis(boronic acid pinacol ester) (39.2 mg, 0.1 mmol), bis(tri-*tert*-butylphosphine)palladium (1.0 mg, 2 × $10^{-3}$ mmol), and 1 drop of Aliquat 336. The tube was sealed and flushed with argon, and then degassed toluene (1.5 mL) and degassed aqueous 2 M $K_2CO_3$ (0.4 mL) were added. The solution was thoroughly degassed under argon, the argon inlet was removed, and the reaction was heated for 3 days at 120 °C (oil bath temperature). After being cooled to room temperature, the mixture was poured into a mixture of methanol (50 mL) and concentrated HCl (10 mL). The precipitant was filtered through a Soxhlet thimble. The polymer was purified by Soxhlet extraction with methanol, acetone, hexane, and chloroform. The chloroform solution was concentrated and precipitated into methanol, and the precipitant was filtered and dried under vacuum to afford PCPDSBT as a dark green solid (72 mg, yield 83%). GPC (chlorobenzene, 80 °C): $M_n$ = 75000 g/mol, $M_w$ = 158000 g/mol; $\lambda_{max}$(film) = 860 nm. $^1$H NMR (*d*-1,1,2,2-tetrachloroethane, 400 MHz, 130 °C): $\delta$ (ppm) 8.16 (s, br, 2H), 7.93 (s, br, 2H), 2.13 (m, br, 4H), 1.39−1.30 (m, br, 52H), 0.98−0.95 (m, br, 10H). Anal. Calcd for $(C_{47}H_{70}N_2SSe_2)_n$: C, 66.17; H, 8.27; N, 3.28. Found: C, 65.05; H, 8.16; N, 3.63.

*(5-Bromoselenophen-2-yl)trimethylsilane (**6**).* To a solution of 2,5-dibromoselenophene (10.8 g, 37.3 mmol) in THF (100 mL) at −78 °C was added a solution of *n*-BuLi (15.7 mL of a 2.5 M solution in hexane, 39.2 mmol) dropwise. After the resulting mixture was stirred for 20 min at this temperature, chlorotrimethylsilane (5.7 mL, 44.8 mmol) was added in one portion. The mixture was allowed to warm to room temperature, water (100 mL) was added, and the mixture was extracted (3 × 100 mL of hexane). The combined organics were dried by $MgSO_4$, filtered, and concentrated under reduced pressure. The residue was purified by silica gel chromatography (eluent hexane) to afford a pale yellow oil (8.6 g, yield 82%). $^1$H NMR ($CDCl_3$, 400 MHz): $\delta$ (ppm) 7.30 (dd, $J$ = 3.7, 1.2 Hz, 2H), 7.22 (dd, $J$ = 3.7, 1.2 Hz, 2H), 0.33 (s, 9H). $^{13}$C NMR ($CDCl_3$, 100 MHz): $\delta$ (ppm) 152.0, 136.4, 134.6, 119.8, 0.17. HRMS (EI$^+$): calcd for $C_7H_{11}BrSeSi$, 281.8979; found, 281.8968.

*(5,5′-(2,5-Dibromo-1,4-phenylene)bis(4-bromoselenophene-5,2-diyl))bis(trimethylsilane) (**8**).* To a solution of (5-bromoselenophen-2-yl)trimethylsilane (3.6 g, 12.8 mmol) in THF (100 mL) at −78 °C was added a solution of lithium diisopropylamide (LDA) (7.7 mL of a 2 M solution in THF/heptanes/ethylbenzene, 15.4 mmol) dropwise. The mixture was stirred for 1 h at this temperature and then warmed to −40 °C for 20 min. $ZnCl_2$ (24 mL of 0.7 M in THF, 16.8 mmol) was added dropwise and the resulting mixture stirred at this temperature for 30 min. Then the mixture was allowed to warm to 0 °C for 1 h and room temperature for 30 min. 1,4-Dibromo-2,5-diiodobenzene (2.5 g, 5.1 mmol) and $Pd(PPh_3)_4$ (295 mg, 0.26 mmol) were added, and the mixture was heated to 65 °C overnight. The mixture was cooled and passed directly through a silica gel plug (5 cm × 5 cm) (eluent THF). The solvent was removed under reduced pressure, and the residue was purified by silica gel chromatography (eluent hexane and then DCM/hexane = 1/1), followed by recrystallization from ethyl acetate to afford a white solid (2.52 g, yield 62%). $^1$H NMR ($CDCl_3$, 400 MHz): $\delta$ (ppm) 7.68 (s, 2H), 7.46 (s, 2H), 0.36 (s, 18H). $^{13}$C NMR ($CDCl_3$, 100 MHz): $\delta$ (ppm) 150.6, 143.8, 138.8, 138.0, 135.7, 122.5, 113.3, 0.03. Anal. Calcd for $C_{20}H_{22}Br_4Se_2Si_2$: C, 30.17; H, 2.79. Found: C, 30.09; H, 2.86.

*2,7-Bis(trimethylsilyl)-4,9-dihydro-s-indaceno[1,2-b:5,6-b′]bis(selenophene) (**9**).* 5,5′-(2,5-Dibromo-1,4-phenylene)bis(4-bromoselenophene-5,2-diyl))bis(trimethylsilane) (6.5 g, 8.2 mmol), bis-(4,4,5,5-tetramethyl-1,3,2-dioxaborolan-2-yl)methane (6.6 g, 24.6 mmol), and bis(tri-*tert*-butylphosphine)palladium (0.63 g, 1.2 mmol) were added into a 250 mL two-neck round-bottom flask under argon. Then predegassed dioxane (120 mL) and 8 M KOH (3.1 mL, 24.8


DOI: 10.1021/jacs.7b03099
J. Am. Chem. Soc. 2017, 139, 8552−8561

mmol) were added. The mixture was thoroughly degassed under argon and stirred for 24 h at 30 °C. Additional KOH (6.2 mL, 49.6 mmol) was added to the mixture, and the reaction was heated 24 h at 60 °C. Water (100 mL) was added and the mixture extracted (3 × 150 mL of DCM). The combined organics were dried by $MgSO_4$, filtered, and concentrated under reduced pressure. The residue was purified by silica gel chromatography (eluent DCM/hexane = 1/2) to afford an off-white solid (2.1 g, yield 51%). $^1$H NMR ($CDCl_3$, 400 MHz): $\delta$ (ppm) 7.58 (s, 2H), 7.50 (s, 2H), 3.69 (s, 2H), 0.36 (s, 18H). $^{13}$C NMR ($CDCl_3$, 100 MHz): $\delta$ (ppm) 151.5, 150.9, 150.0, 145.1, 138.8, 131.9, 116.6, 34.9, 0.4. TOF MS (ES) [$M^+$]: calcd for $C_{22}H_{26}Se_2Si_2$, 505.9903; found, 505.9915.

*4,4,9,9-Tetrahexadecyl-4,9-dihydro-s-indaceno[1,2-b:5,6-b′]bis(selenophene) (**10**).* To a solution of 2,7-bis(trimethylsilyl)-4,9-dihydro-*s*-indaceno[1,2-*b*:5,6-*b*′]bis(selenophene) (0.51 g, 1.0 mmol) in anhydrous DMSO (40 mL) was added sodium *tert*-butoxide (0.58 g, 6.0 mmol). The mixture was stirred at 70 °C for 30 min before 1-bromohexadecane (1.9 g, 6.2 mmol) was added dropwise. The mixture was heated to 80 °C overnight and poured into ice−water (150 mL). The precipitant was filtered, washed by water and methanol, and dried under vacuum. The solid was purified by silica gel chromatography (eluent hexane) to afford an off-white solid (0.77 g, yield 61%). $^1$H NMR ($CDCl_3$, 400 MHz): $\delta$ (ppm) 7.89 (d, $J$ = 5.3 Hz, 2H), 7.23 (s, 2H), 7.18 (d, $J$ = 5.3 Hz, 2H), 1.99−1.83 (m, 8H), 1.31−1.08 (m, 104H), 0.89−0.78 (m, 20H). $^{13}$C NMR ($CDCl_3$, 100 MHz): $\delta$ (ppm) 156.8, 152.2, 144.4, 138.0, 130.6, 124.2, 113.4, 54.9, 39.1, 31.9, 29.7, 29.7−29.6 (overlapping C), 29.4, 22.7, 14.1. MALDI-TOF: 1259.9 ($M^+$).

*2,7-Dibromo-4,4,9,9-tetrahexadecyl-4,9-dihydro-s-indaceno[1,2-b:5,6-b′]bis(selenophene) (**11**).* To a solution of 4,4,9,9-tetrahexadecyl-4,9-dihydro-*s*-indaceno[1,2-*b*:5,6-*b*′]bis(selenophene) (1.07 g, 0.85 mmol) in THF (50 mL) was added NBS (0.32 g, 1.8 mmol) in one portion at room temperature, and the mixture was stirred for 2 h in the absence of light. The mixture was poured into water (200 mL), and the precipitant was filtered, washed by water and methanol, and dried under vacuum, followed by recrystallization from hexane to afford a pale yellow solid (1.1 g, yield 91%). $^1$H NMR ($CDCl_3$, 400 MHz): $\delta$ (ppm) 7.15 (s, 2H), 7.13 (s, 2H), 1.93−1.79 (m, 8H), 1.31−1.08 (m, 104H), 0.89−0.72 (m, 20H). $^{13}$C NMR ($CDCl_3$, 100 MHz): $\delta$ (ppm) 155.2, 151.2, 145.2, 138.0, 127.5, 115.0, 113.3, 55.8, 39.0, 29.7, 29.7, 29.7−29.6 (overlapping C), 29.4, 23.9, 22.7, 14.1. MALDI-TOF: 1417.9 ($M^+$).

*Poly[4,4,9,9-tetrahexadecyl-4,9-dihydro-s-indaceno[1,2-b:5,6-b′]-bis(selenophene)-2,7-diyl-alt-(2,1,3-benzothiadiazole)-4,7-diyl] (PIDSeBT).* A 20 mL high-pressure microwave reactor tube was charged with 2,7-dibromo-4,4,9,9-tetrahexadecyl-4,9-dihydro-*s*-indaceno[1,2-*b*:5,6-*b*′]bis(selenophene) (565.0 mg, 0.40 mmol), 2,1,3-benzothiadiazole-4,7-bis(boronic acid pinacol ester) (154.9 mg, 0.40 mmol), $Pd_2(dba)_3$ (5.5 mg, $6 \times 10^{-3}$ mmol), P-(*o*-tol)$_3$ (7.3 mg, 0.024 mmol), and 3 drops of Aliquat 336. The tube was sealed and flushed with argon, and then degassed toluene (10 mL) and degassed aqueous 1 M $Na_2CO_3$ (2 mL) were added. The solution was thoroughly degassed under argon, the argon inlet was removed, and the reaction heated for 2 days at 120 °C (oil bath temperature). After being cooled to room temperature, the mixture was poured into a mixture of methanol (100 mL) and concentrated HCl (20 mL). The precipitant was filtered through a Soxhlet thimble. The polymer was purified by Soxhlet extraction with methanol, acetone, hexane, and chloroform. The chloroform solution was concentrated and precipitated into methanol, and the precipitant was filtered and dried under vacuum to afford PIDSeBT as a dark green solid (476 mg, yield 86%). GPC (chlorobenzene, 80 °C): $M_n$ = 119000 g/mol, $M_w$ = 303000 g/mol; $\lambda_{max}$(film) = 725 nm. $^1$H NMR (*d*-1,1,2,2-tetrachloroethane, 400 MHz, 130 °C): $\delta$ (ppm) 8.17 (s, br, 2H), 7.97 (s, br, 2H), 7.45 (s, br, 2H), 2.18−2.10 (m, br, 8H), 1.40−1.26 (m, br, 104H), 0.97−0.94 (m, br, 20H). Anal. Calcd for $(C_{86}H_{138}N_2SSe_2)_n$: C, 74.31; H, 10.01; N, 2.02. Found: C, 74.15; H, 10.15; N, 2.14.

## RESULTS AND DISCUSSION

**Synthesis and Characterization.** The most common routes to alkylated thiophene-based ladder monomers of cyclopentadithiophene (CDT) and indacenodithiophene (IDT) usually involve alkylation of the methylene (−$CH_2$−)-bridged precursor. However, the synthesis of this key intermediate often involves relatively harsh reaction conditions, for example, an acid-catalyzed Freidel−Crafts acylation, followed by reduction of the resulting ketone.[51−54] Such sequences are usually low yielding for thiophene-based materials, due to the high reactivity of thiophene under acidic conditions and due to difficulties in purifying the poorly soluble fused ketone intermediates. These routes thus appeared even more unattractive for the selenophene analogues, particularly given the higher reactivity of selenophene over thiophene. We therefore developed a route directly to the methylene-bridged intermediates that avoided acidic conditions (Scheme 1) and utilized a Suzuki ring closing of a suitable di- or tetrabromo derivative with bis(4,4,5,5-tetramethyl-1,3,2-dioxaborolan-2-yl)-methane.[44,55−58]

Hence, previously unknown cyclopentadiselenophene (CPDS, **2**) was isolated in 37% yield from **1**, following ring closure with Pd[P-(*t*-Bu)$_3$]$_2$ in a mixture of dioxane/aqueous KOH with Pd[P-(*t*-Bu)$_3$]$_2$. In this case the crude product was directly desilylated with TBAF before isolation to avoid complications with partial loss of the trimethylsilyl groups during chromatography. Subsequent alkylation with 1-bromohexadecane followed by bromination with NBS afforded monomer material **4** in 66% yield over the two steps. Gratifyingly, such an approach was even successful for the more challenging 4-fold cross-coupling of tetrabromo derivative **8** (itself prepared from 2,5-dibromoselenophene in three steps in 51% yield) to afford the new 4,9-dihydro-*s*-indaceno[1,2-*b*:5,6-*b*′]bis(selenophene) (IDSe) in 51% yield. The higher yield compared to that of CPDS, despite the 4-fold coupling, is likely related to the very electron rich nature of **1** compared to **8**. This different electron densities of the ring-closed monomers is also reflected in the fact that the silylated IDSe was stable during chromatography, unlike CPDS, which was partially desilyated. The IDSe was readily alkylated with hexadecyl side chains and brominated in an overall yield of 55%.

Our initial attempts to prepare the copolymer of dibrominated CPDS (**4**) and 2,1,3-benzothiadiazole-4,7-bis-(boronic acid pinacol ester) under standard Suzuki polymerization conditions with Pd(PPh$_3$)$_4$ or $Pd_2(dba)_3$/P-(*o*-tol)$_3$ as the catalyst were unsuccessful. Only very low weight oligomer material was formed. We believed this related to problems with the oxidative addition of the catalyst to the very electron rich CPDS. Therefore, use of the more reactive catalyst Pd[P-(*t*-Bu)$_3$]$_2$ enabled the successful isolation of polymeric material. Unlike PCPDSBT, PIDSeBT was readily prepared by $Pd_2$-$(dba)_3$/P-(*o*-tol)$_3$ as the catalyst under standard Suzuki polymerization conditions. Both polymers were purified by precipitation into acidic methanol followed by Soxhlet extraction with methanol, acetone, hexane, and chloroform. PCPDSBT and PIDSeBT were obtained as dark green solids in yields of 83% and 86%, respectively. Both polymers exhibited good solubility in common organic solvents, such as chloroform, toluene, chlorobenzene, etc.

**Physical and Optoelectronic Properties.** Both PCPDSBT and PIDSeBT exhibited good thermal stabilities, as evaluated by thermal gravimetric analysis (TGA) (Figure


DOI: 10.1021/jacs.7b03099
J. Am. Chem. Soc. 2017, 139, 8552−8561

**Scheme 1. Synthetic Route to Monomers and Polymers**

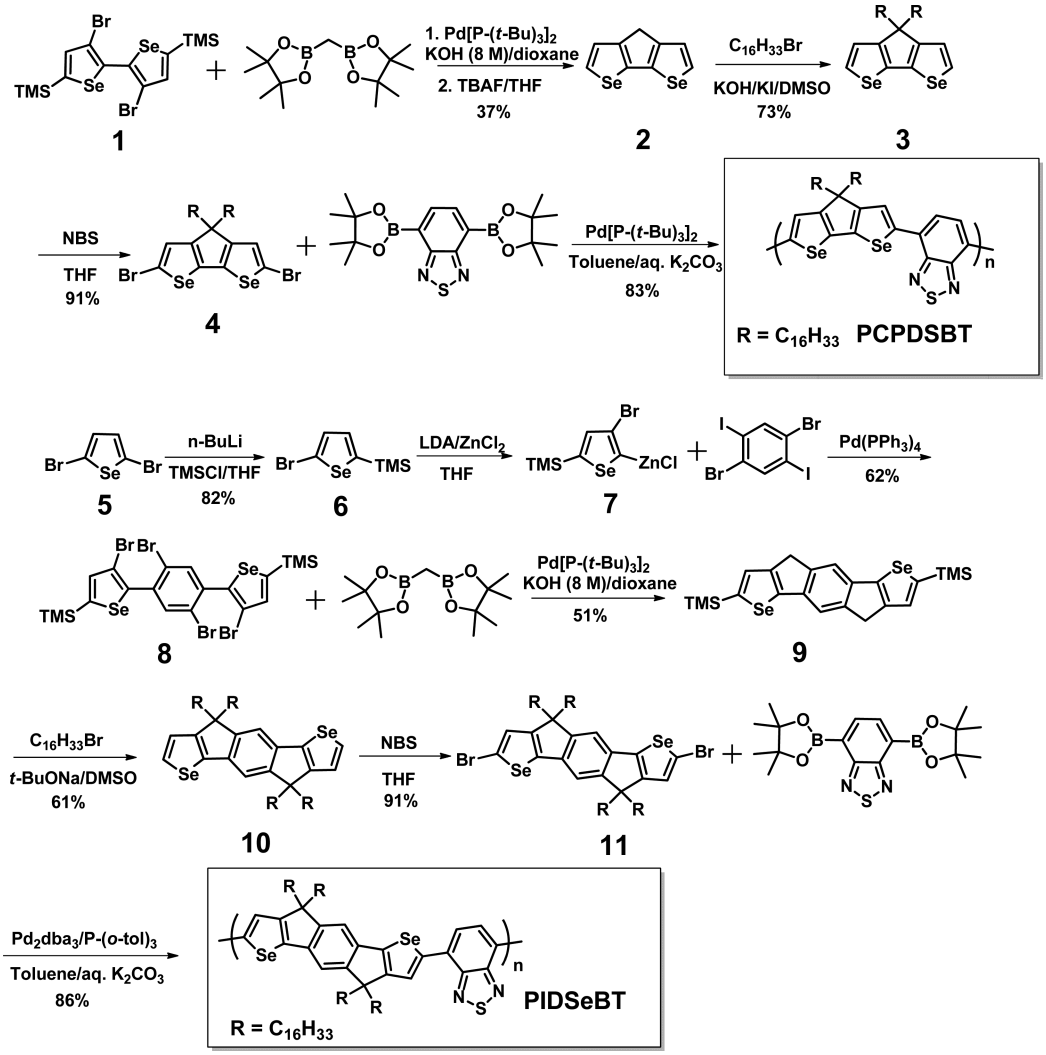


S1a, Supporting Information), with a 5% weight loss at temperatures of 390 and 410 °C under nitrogen, respectively. Differential scanning calorimetry (DSC) curves (Figure S1b) of both polymers showed no obvious thermal transitions upon cycling between 0 and 300 °C, suggesting, in agreement with many ladder polymers, that the backbone melting temperature is above 300 °C. DFT calculations of trimers of PCPDSBT and PIDSeBT were modeled using Gaussian at the B3LYP/6-31G* level, with the side chains modified to an ethyl group for simplifying the calculations. The minimum-energy conformations of the CPDSBT and IDSeBT trimers both show the polymers adopt almost coplanar backbones (Figure 1), potentially minimizing torsional disorder along the backbone.[59] The minimum-energy conformation of CPDSBT also shows PCPDSBT has a slightly flexural geometry, which potentially hinders the charge transport along the backbone.[60,61] However, that of IDSeBT exhibits a more linear geometry, which may facilitate charge transport. Both the highest occupied molecular orbital (HOMO) and the lowest unoccupied molecular orbital (LUMO) of PCPDSBT are predicted to be delocalized over the entire backbones, while the HOMO of PIDSeBT is delocalized and the LUMO is mainly localized on the acceptor unit (Figures S2 and S3, Supporting Information).

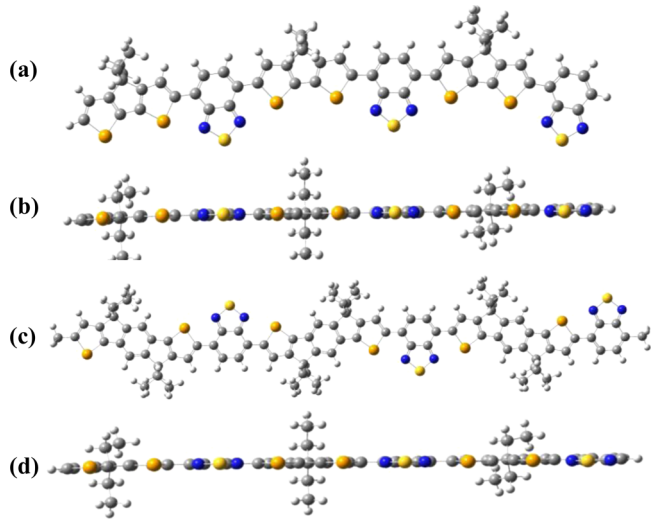


**Figure 1.** Energy-minimized structures of the ethyl-substituted CPDSBT trimer (a, top view; b, side view) and IDSeBT trimer (c, top view; d, side view) calculated using DFT at the B3LYP/6.31G* level.



DOI: 10.1021/jacs.7b03099
J. Am. Chem. Soc. 2017, 139, 8552−8561

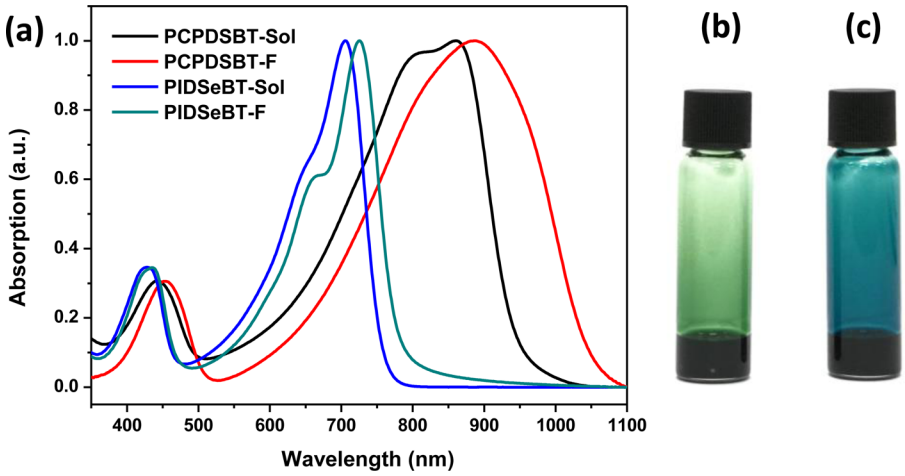


**Figure 2.** (a) UV−vis absorption spectra of PCPDSBT and PIDSeBT in dilute tetralin and as spin-cast thin films. Images of PCPDSBT (b) and PIDSeBT (c) in tetralin at 10 mg/mL at room temperature.

**Table 1. Physical Properties of PCPDSBT and PIDSeBT**

| | $M_n$[a] (KDa) | $M_w$[a] (KDa) | $Đ$ | UV(sol) peaks (nm) | UV(film) peaks (nm) | onset (nm) | $E_{g,opt}$[b] (eV) | IP[c] (eV) |
|---|---|---|---|---|---|---|---|---|
| PCPDSBT | 75 | 158 | 2.1 | 443, 806, 860 | 455, 885 | 1050 | 1.18 | 4.85 |
| PIDSeBT | 119 | 303 | 2.5 | 426, 650, 705 | 434, 663, 725 | 780 | 1.59 | 5.22 |

[a]Measured using gel permeation chromatography (against polystyrene standards) in chlorobenzene at 80 °C. [b]Optical band gap estimated from the low-energy band edge in the optical spectrum. [c]Ionization potential measured by UV−PESA (error ±0.05 eV).

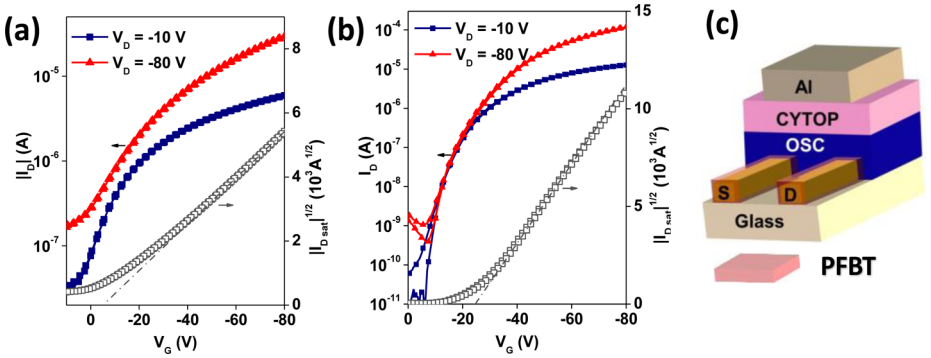


**Figure 3.** Typical transfer characteristics of the BC/TG configuration OTFT device with PCPDSBT/PFBT (a) and PIDSeBT/PFBT (b) annealed at 200 °C. (c) Device structure employed.

The UV−vis absorption spectra of PCPDSBT and PIDSeBT in dilute tetralin and as thin films are shown in Figure 2 and the data summarized in Table 1. PCPDSBT exhibits two main broad absorption bands in dilute tetralin, with a peak of 443 nm in the high-energy region which is assigned to $\pi-\pi^*$ transitions of the main backbone and a peak of 860 nm with a shoulder of 806 nm in the low-energy region which we attribute to an intramolecular charge transfer (ICT) from the CPDS donor to the BT acceptor. In the film, the main peaks of PCPDSBT are red-shifted to 455 and 885 nm, suggestive of backbone planarization and ordering in the solid state. The long-wavelength peak is red-shifted by around 135 nm compared to that of its thiophene analogue CDT−BT,[62] further demonstrating the significant impact of selenophene substitution on the optical spectra.[17,27,63−69] The absorption onset of PCPDSBT in the solid state is around 1050 nm, corresponding to an optical band gap of 1.18 eV, which is among the lowest reported for donor−acceptor polymers.[70−75] PIDSeBT also exhibits two main bands with peaks at 426, 650, and 705 nm in tetralin solution and 434, 663, and 725 nm in the solid state. The absorption onset of PIDSeBT in the solid state is 780 nm, corresponding to an optical band gap of 1.59 eV. The band gap of PCPDSBT is much smaller than that of PIDSeBT, which can be attributed to enhanced ICT from the stronger donor unit CPDS to the BT acceptor unit. The ionization potentials (IPs) of thin films of PCPDSBT and PIDSeBT were measured by PESA to be 4.85 and 5.22 eV, respectively. The IP of PIDSeBT is around 0.18 eV smaller than that of the thiophene analogue measured by the same technique.[54]

**Thin-Film Transistor Properties.** The charge transport properties of both polymers were assessed in bottom-contact/top-gate (BC/TG) TFTs. Importantly, both polymers were deposited from tetralin solutions, thereby avoiding the use of hazardous chlorinated solvents. Polymers were spin coated onto glass substrates equipped with prepatterned Au source/drain electrodes, which were treated with the PFBT self-assembling monolayer to improve hole injection, followed by annealing at 200 °C. Both PCPDSBT and PIDSeBT displayed dominant p-type behavior, with negligible hysteresis between


DOI: 10.1021/jacs.7b03099
J. Am. Chem. Soc. 2017, 139, 8552−8561

the forward and reverse bias transfer characteristics (Figure 3; Figure S4, Supporting Information). PCPDSBT exhibited the lower performance of the two polymers with average linear and saturation mobilities of 0.10 and 0.14 $cm^2\ V^{-1}\ s^{-1}$, respectively. Although these values are lower than those reported previously for the best performing thiophene analogues,[13,76−78] we note that these were only achieved with carefully optimized processing (chain alignment techniques) and molecular weight. In comparison, transistors based on PIDSeBT performed significantly better, with average linear and saturation mobility values of 0.56 and 1.6 $cm^2\ V^{-1}\ s^{-1}$, respectively.

On the basis of these initial results, we further optimized the PIDSeBT transistors via a combination of postdeposition thermal treatment and interfacial layer engineering. The use of a higher annealing temperature of 270 °C was found to enhance the performance (Table 2; Figure S5, Supporting Information), with the hole mobility, measured in saturation, now reaching 2.8 $cm^2\ V^{-1}\ s^{-1}$. Interestingly, the threshold gate voltage in these devices was also found to increase by 7−8 V, as compared to those of transistors annealed at 200 °C, suggesting a higher injection barrier for holes, possibly a result of PFBT desorption from the Au electrode. In an effort to address this issue, the PFBT monolayer was replaced with a thin layer of solution-processed CuSCN. The role of the later material is twofold: first, it provides a more thermally stable layer than PFBT, and second, it acts as a highly effective electron-blocking layer while enhancing hole injection.[10,79,80] The transfer and output characteristics of the resulting OTFT are shown in Figures 4 and S5. The average saturation mobility of the PIDSeBT transistors featuring the CuSCN interlayer annealed at 200 °C was 1.8 $cm^2\ V^{-1}\ s^{-1}$, a slightly higher value than that measured for the PFBT/Au-based device annealed at the same temperature. However, devices annealed at 270 °C yielded a significantly higher hole mobility of 4.4 $cm^2\ V^{-1}\ s^{-1}$ with a remarkable maximum value of 6.4 $cm^2\ V^{-1}\ s^{-1}$. Notably, the linear mobilities of the CuSCN/Au device are significantly higher than those of the PFBT/Au-based device, while the threshold voltages of the former were lower than those of the latter—both indicating an improved matching between the work function of CuSCN/Au and the HOMO level of PIDSeBT.[10] This was manifested by a 3-fold reduction in the contact resistance of the CuSCN/Au devices compared to that of PFBT/Au devices at $V_D$ = −80 V (Figure S6, Supporting Information). We note that the mobility values obtained here are among the highest reported to date for polymers processed via spin-coating from a nonchlorinated solvent without the use of any special alignment techniques.[35] Most importantly, optimized devices exhibit excellent transfer characteristics without the undesirable peak in mobility often observed at low gate voltages due to parasitic contact resistance.

The subthreshold regime of the devices was also investigated to determine whether the performance improvement was due to decreasing trap density within the bulk film as a result of thermal annealing or the employment of the hole injection layer. The deep trap density in the bulk film displayed a negligible difference for all PIDSeBT-based devices, in the range of $(0.9–1.3) \times 10^{12}\ eV^{-1}\ cm^{-2}$ (Table S1, Supporting Information). Thus, the increase in mobility is most likely attributed to local changes at the semiconductor/dielectric interface and/or molecular rearrangement and the improved hole injection characteristics.

**Morphological Characterization.** The organization of polymer chains down to the molecular level was studied with GIWAXS (see Figure 5). The two-dimensional GIWAXS image of PCPDSBT is similar in many regards to that of CDT−BT.[81,82] Three orders of alkyl (lamellar) stacking peaks are seen along $q_z$, with some alkyl stacking peaks also observed in-plane (along $q_{xy}$), indicating a mixture of "edge-on"- and "face-on"-oriented chains. The first-order lamellar stacking peak is observed at $q \approx 2.4\ nm^{-1}$, giving an alkyl stacking distance of ~2.6 nm consistent with that found for CDT−BT.[81] A $\pi$−$\pi$ stacking peak is found at a value of $q \approx 16.5\ nm^{-1}$ corresponding to a $\pi$−$\pi$ stacking distance of 0.38 nm, also

**Table 2. OTFT Device Performance of PCPDSBT and PIDSeBT in Bottom-Gate/Top-Contact Devices**

| polymer[a] | $\mu_{sat}$(av) ($\mu_{sat}$(max)) ($cm^2\ V^{-1}\ s^{-1}$) | $\mu_{lin}$(av) ($cm^2\ V^{-1}\ s^{-1}$) | $V_{Th}$ (V) | $I_{on}/I_{off}$ |
|---|---|---|---|---|
| PIDSeBT/PFBT_270 | 2.8 (3.2) | 0.58 | −34.0 | $10^5$−$10^6$ |
| PIDSeBT/CuSCN_270 | 4.4 (6.4) | 1.8 | −24.8 | $10^5$−$10^6$ |
| PIDSeBT/PFBT_200 | 1.6 (1.7) | 0.56 | −26.9 | $10^5$−$10^6$ |
| PIDSeBT/CuSCN_200 | 1.8 (2.0) | 1.1 | −21.3 | $10^5$−$10^6$ |
| PCPDSBT/PFBT_200 | 0.14 (0.15) | 0.10 | −5.0 | ~$10^2$ |

[a]The compound after the slash indicates the monolayer material, and the number after the underscore indicates the annealing temperature (°C).

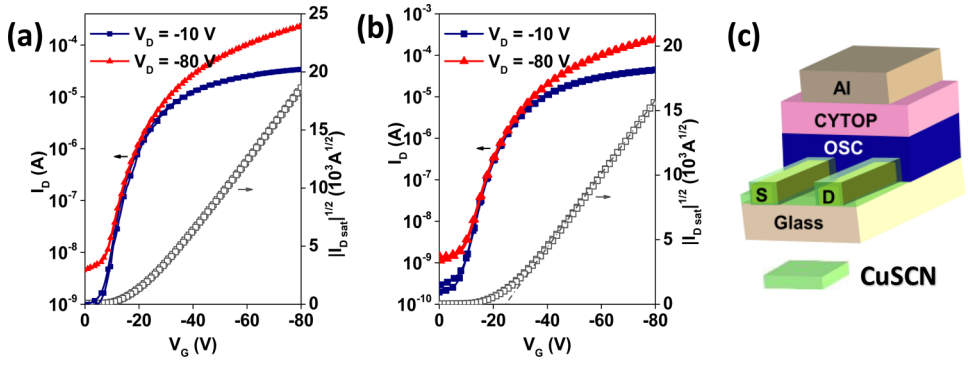


**Figure 4.** Typical transfer characteristics of the BC/TG configuration OTFT device with PIDSeBT/CuSCN annealed at 200 °C (a) and 270 °C (b). (c) Device structure employed.



DOI: 10.1021/jacs.7b03099
J. Am. Chem. Soc. 2017, 139, 8552−8561

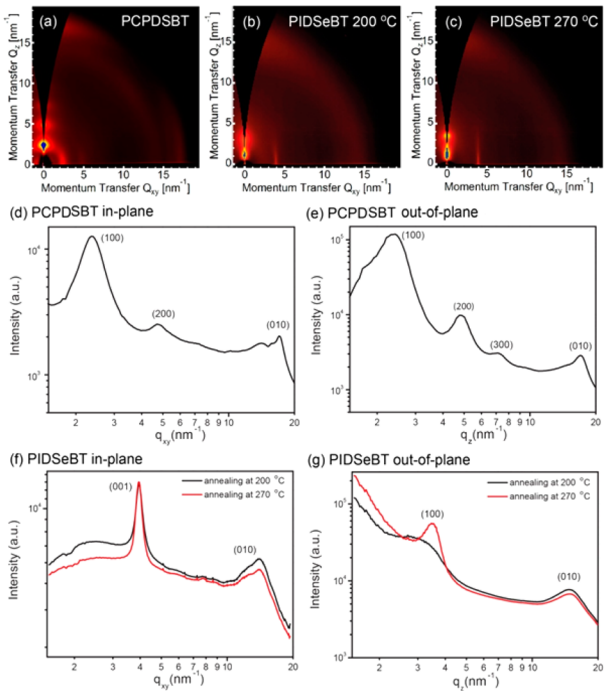


**Figure 5.** Two-dimensional GIWAXS images of PCDPSBT annealed at 200 °C (a), PIDSeBT annealed at 200 °C (b), and PIDSeBT annealed at 270 °C (c). Also shown are one-dimensional scattering profiles taken along the in-plane (d, f) and out-of-plane (e, g) directions for PCPDSBT (d, e) and PIDSeBT (f, g).

consistent with values reported for CDT−BT.[81,82] The scattering pattern of PCPDSBT also shows a broad feature located at $q \approx 14$ nm$^{-1}$ that is most intense at $\sim(q_{xy}, q_z) = (10$ nm$^{-1}$, 10 nm$^{-1}$), which is associated with the ordered stacking of the side chains.[81] Thus, PCPDSBT is very similar in its packing to CDT−BT, with the exchange of sulfur atoms for selenium atoms only slightly perturbing the microstructure. The lower OTFT performance of PCPDSBT observed here compared to values previously reported for CDT−BT may be due to suboptimal processing,[82] with the mixture of face-on and edge-on components seen here less than ideal. Table 3 summarizes the crystallographic spacings and coherence lengths determined from the GIWAXS data.

In contrast to PCPDSBT, PIDSeBT shows a very different molecular packing. The 2D GIWAXS images of the PIDSeBT films are characterized by a prominent backbone stacking (001) peak located in-plane at $q = 3.95$ nm$^{-1}$. This peak is distinguished from an alkyl stacking peak by its narrow, vertical shape and corresponds to a backbone repeat distance of 1.59 nm. A weak alkyl stacking peak is seen in the out-of-plane direction, corresponding to a $d$-spacing of ∼1.8 nm, which is very different from the much larger spacing seen for PCPDSBT. The $\pi-\pi$ stacking distance of PIDSeBT is found to be ∼0.42 nm, slightly larger than the value measured for IDT−BT.[54] The shorter lamellar spacing and larger $\pi-\pi$ spacing of PIDSeBT compared to PCPDSBT indicate that PIDSeBT adopts a completely different side-chain-packing geometry. Indeed, the rigid, planar nature of the PIDSeBT backbone promotes backbone ordering over side-chain ordering. High degrees of order in lamellar stacking have been shown not to be necessary for high charge transport mobility, with polymers such as IDT−BT demonstrating exceptionally low degrees of energetic disorder attributed to their backbone planarity.[59] With the increase in annealing temperature from 200 to 270 °C, the crystalline features of PIDSeBT become sharper, notably the backbone stacking peak, which helps to understand the increase in mobility with annealing in terms of improved order along the polymer backbone.

To probe the surface microstructures, the morphologies of the polymer semiconductor films were characterized by tapping mode AFM. Sample films were prepared under conditions identical to those of OTFT fabrication except that no dielectric or gate electrodes were deposited. The topography and phase images of polymer films processed under different conditions are shown in Figures 6 and S7 (Supporting Information). PCPDSBT forms a continuous and smooth film with fine fibrillar structures, affording surface roughness (root-mean-square, rms) of 0.649 nm after annealing at 200 °C. PIDSeBT yielded films with less pronounced microstructural features, and a similar rms of 0.748 nm. The film turned modestly smoother after annealing at a higher temperature of 270 °C, with an rms of 0.560 nm. Films cast atop CuSCN and annealed at 200 °C were rougher than those without an interfacial layer, with an rms of 1.326 nm, due to the rather rough surface of crystallized CuSCN.[83] The surface roughness decreased to 0.582 nm after annealing at 270 °C, in agreement with the increase in transistor performance.

## CONCLUSION

In conclusion, we have reported the synthesis of two novel selenophene-containing ladder monomers by a 2-fold and 4-fold Pd-catalyzed ring-closing reaction between bis(4,4,5,5-tetramethyl-1,3,2-dioxaborolan-2-yl)methane and the di- and tetrabrominated aryl precursors. This route, which avoids the necessity for harsh acidic or reducing conditions, allows the preparation of unalkylated cyclopentadiselenophene (CPDS) and indacenodiselenophene (IDSe) for the first time. Subsequent alkylation with long hexadecyl side chains affords highly soluble monomeric materials, which were copolymerized with the electron acceptor benzothiadiazole. The resulting polymers PCPDSBT and PIDSeBT exhibit highly coplanar backbones in combination with excellent solubility in a range of nonchlorinated solvents. The optical band gap of PCPDSBT exhibits a significant red shift compared to that of the well-investigated thiophene analogue, with a small optical band gap of 1.18 eV, one of the lowest reported for a donor−acceptor copolymer. Thin-film transistors fabricated from tetralin solutions of both polymers exhibited p-type behavior, with PIDSeBT exhibiting a hole mobility up to 6.4 cm$^2$ V$^{-1}$ s$^{-1}$ after

**Table 3. Crystallographic Spacings and Coherence Lengths Determined from the GIWAXS Data**

| polymer | (100) $d$-spacing (nm) | (100) coherence length (nm) | (010) $d$-spacing (nm) | (010) coherence length (nm) | (001) $d$-spacing (nm) | (001) coherence length (nm) |
|---|---|---|---|---|---|---|
| PCPDSBT | 2.60 | 13.4 | 0.38 | 9.1 | | |
| PIDSeBT (200 °C) | | | 0.42 | 2 | 1.59 | 18.8 |
| PIDSeBT (270 °C) | 1.79 | 10.6 | 0.42 | 2 | 1.59 | 21.6 |


DOI: 10.1021/jacs.7b03099
J. Am. Chem. Soc. 2017, 139, 8552−8561

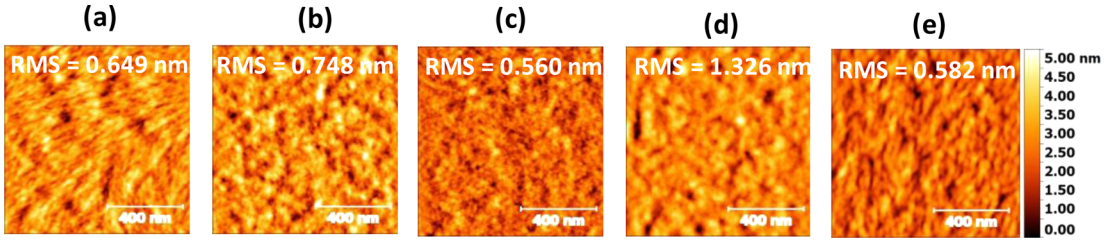


**Figure 6.** AFM topography images of polymer films: (a) PCPDSBT on glass annealed at 200 °C, (b) PIDSeBT on glass annealed at 200 °C, (c) PIDSeBT on glass annealed at 270 °C, (d) PIDSeBT on a CuSCN surface annealed at 200 °C, (e) PIDSeBT on a CuSCN surface annealed at 270 °C. All images are 1 × 1 $\mu m^2$.

device optimization. This is among the best reported transistor performances for a polymer fabricated from a nonchlorinated solvent. Importantly, these devices exhibited excellent transfer characteristics without the undesirable peak in mobility often observed at low gate voltages due to parasitic contact resistance. These results demonstrate that the incorporation of selenophene into ladder-type structures is a possible route to improve the performance of the materials. In particular, given the interest in ladder-type monomers for non-fullerene acceptor materials, we believe that this synthetic approach will be of further interest for the development of new types of acceptor backbones.

## ■ ASSOCIATED CONTENT

### Supporting Information

The Supporting Information is available free of charge on the ACS Publications website at DOI: 10.1021/jacs.7b03099.

TGA plots, DSC traces, modeling, transistor plots, and AFM data (PDF)

## ■ AUTHOR INFORMATION


### Corresponding Authors

*yang.han@imperial.ac.uk
*m.heeney@imperial.ac.uk

### ORCID

Christopher R. McNeill: 0000-0001-5221-878X
Martin Heeney: 0000-0001-6879-5020


### Notes

The authors declare no competing financial interest.

Additional data relating to the paper can be found at dx.doi.org/10.6084/m9.figshare.5001965.

## ■ ACKNOWLEDGMENTS

We thank the British Council (Grant No. 173601536) and Engineering and Physical Sciences Research Council (EPSRC) (Grant No. EP/L016702/1) for support. C.R.M. acknowledges support from the Australian Research Council (Grant No. DP130102616). This research was undertaken in part on the SAXS/WAXS beamline at the Australian Synchrotron, Victoria, Australia.

## ■ REFERENCES


(1) Yi, Z.; Wang, S.; Liu, Y. *Adv. Mater.* **2015**, *27*, 3589.
(2) Lu, L.; Zheng, T.; Wu, Q.; Schneider, A. M.; Zhao, D.; Yu, L. *Chem. Rev.* **2015**, *115*, 12666.
(3) Chen, Q.; Zhang, Q. *J. Mater. Chem. C* **2017**, *5*, 1275.
(4) Guo, X.; Facchetti, A.; Marks, T. J. *Chem. Rev.* **2014**, *114*, 8943.
(5) Sirringhaus, H. *Adv. Mater.* **2014**, *26*, 1319.
(6) Zhang, L.; Cao, Y.; Colella, N. S.; Liang, Y.; Brédas, J.-L.; Houk, K. N.; Briseno, A. L. *Acc. Chem. Res.* **2015**, *48*, 500.
(7) Wu, J.-S.; Cheng, S.-W.; Cheng, Y.-J.; Hsu, C.-S. *Chem. Soc. Rev.* **2015**, *44*, 1113.
(8) Holliday, S.; Donaghey, J.; McCulloch, I. *Chem. Mater.* **2014**, *26*, 647.
(9) He, M.; Li, W.; Gao, Y.; Tian, H.; Zhang, J.; Tong, H.; Yan, D.; Geng, Y.; Wang, F. *Macromolecules* **2016**, *49*, 825.
(10) Zhang, W.; Han, Y.; Zhu, X.; Fei, Z.; Feng, Y.; Treat, N. D.; Faber, H.; Stingelin, N.; McCulloch, I.; Anthopoulos, T. D.; Heeney, M. *Adv. Mater.* **2016**, *28*, 3922.
(11) Li, Y.; Yao, K.; Yip, H. L.; Ding, F. Z.; Xu, Y. X.; Li, X.; Chen, Y.; Jen, A. K.-Y. *Adv. Funct. Mater.* **2014**, *24*, 3631.
(12) Luo, C.; Kyaw, A. K. K.; Perez, L. A.; Patel, S.; Wang, M.; Grimm, B.; Bazan, G. C.; Kramer, E. J.; Heeger, A. J. *Nano Lett.* **2014**, *14*, 2764.
(13) Yamashita, Y.; Hinkel, F.; Marszalek, T.; Zajaczkowski, W.; Pisula, W.; Baumgarten, M.; Matsui, H.; Müllen, K.; Takeya, J. *Chem. Mater.* **2016**, *28*, 420.
(14) Zhang, X.; Bronstein, H.; Kronemeijer, A. J.; Smith, J.; Kim, Y.; Kline, R. J.; Richter, L. J.; Anthopoulos, T. D.; Sirringhaus, H.; Song, K.; Heeney, M.; Zhang, W.; McCulloch, I.; DeLongchamp, D. M. *Nat. Commun.* **2013**, *4*, 2238.
(15) Lee, B. H.; Bazan, G. C.; Heeger, A. J. *Adv. Mater.* **2016**, *28*, 57.
(16) Lee, B. H.; Hsu, B. B. Y.; Patel, S. N.; Labram, J.; Luo, C.; Bazan, G. C.; Heeger, A. J. *Nano Lett.* **2016**, *16*, 314.
(17) Fei, Z.; Ashraf, R. S.; Han, Y.; Wang, S.; Yau, C. P.; Tuladhar, P. S.; Anthopoulos, T. D.; Chabinyc, M. L.; Heeney, M. *J. Mater. Chem. A* **2015**, *3*, 1986.
(18) Ashraf, R. S.; Meager, I.; Nikolka, M.; Kirkus, M.; Planells, M.; Schroeder, B. C.; Holliday, S.; Hurhangee, M.; Nielsen, C. B.; Sirringhaus, H.; McCulloch, I. *J. Am. Chem. Soc.* **2015**, *137*, 1314.
(19) Kang, I.; Yun, H.; Chung, D. S.; Kwon, S.; Kim, Y. *J. Am. Chem. Soc.* **2013**, *135*, 14896.
(20) Intemann, J. J.; Yao, K.; Yip, H.; Xu, Y.; Li, Y.; Liang, P.; Ding, F.; Li, X.; Jen, A. K.-Y. *Chem. Mater.* **2013**, *25*, 3188.
(21) Back, J. Y.; Yu, H.; Song, I.; Kang, I.; Ahn, H.; Shin, T. J.; Kwon, S. K.; Oh, J. H.; Kim, Y. H. *Chem. Mater.* **2015**, *27*, 1732.
(22) Zhao, Z.; Yin, Z.; Chen, H.; Zheng, L.; Zhu, C.; Zhang, L.; Tan, S.; Wang, H.; Guo, Y.; Tang, Q.; Liu, Y. *Adv. Mater.* **2017**, *29*, 1602410.
(23) Shahid, M.; McCarthy-Ward, T.; Labram, J.; Rossbauer, S.; Domingo, E. B.; Watkins, S. E.; Stingelin, N.; Anthopoulos, T. D.; Heeney, M. *Chem. Sci.* **2012**, *3*, 181.
(24) Kronemeijer, A. J.; Gili, E.; Shahid, M.; Rivnay, J.; Salleo, A.; Heeney, M.; Sirringhaus, H. *Adv. Mater.* **2012**, *24*, 1558.
(25) Jung, E. H.; Bae, S.; Yoo, T. W.; Jo, W. H. *Polym. Chem.* **2014**, *5*, 6545.
(26) Al-Hashimi, M.; Han, Y.; Smith, J.; Bazzi, H. S.; Alqaradawi, S. Y. A.; Watkins, S. E.; Anthopoulos, T. D.; Heeney, M. *Chem. Sci.* **2016**, *7*, 1093.
(27) Saadeh, H. a; Lu, L.; He, F.; Bullock, J. E.; Wang, W.; Carsten, B.; Yu, L. *ACS Macro Lett.* **2012**, *1*, 361.
(28) Hwang, Y.; Ren, G.; Murari, N. M.; Jenekhe, S. A. *Macromolecules* **2012**, *45*, 9056.




DOI: 10.1021/jacs.7b03099
J. Am. Chem. Soc. 2017, 139, 8552−8561

(29) Conboy, G.; Spencer, H. J.; Angioni, E.; Kanibolotsky, A. L.; Findlay, N. J.; Coles, S. J.; Wilson, C.; Pitak, M. B.; Risko, C.; Coropceanu, V.; Brédas, J.-L.; Skabara, P. J. *Mater. Horiz.* **2016**, *3*, 333.
(30) Tsai, C.; Fortney, A.; Qiu, Y.; Gil, R. R.; Yaron, D.; Kowalewski, T.; Noonan, K. J. T. *J. Am. Chem. Soc.* **2016**, *138*, 6798.
(31) Gao, D.; Gibson, G. L.; Hollinger, J.; Li, P.; Seferos, D. S. *Polym. Chem.* **2015**, *6*, 3353.
(32) Yan, H.; Hollinger, J.; Bridges, C. R.; Mckeown, G. R.; Al-faouri, T.; Seferos, D. S. *Chem. Mater.* **2014**, *26*, 4605.
(33) Alghamdi, A. a. B.; Watters, D. C.; Yi, H.; Al-Faifi, S.; Almeataq, M. S.; Coles, D.; Kingsley, J.; Lidzey, D. G.; Iraqi, A. *J. Mater. Chem. A* **2013**, *1*, 5165.
(34) Sung, M. J.; Luzio, A.; Park, W. T.; Kim, R.; Gann, E.; Maddalena, F.; Pace, G.; Xu, Y.; Natali, D.; de Falco, C.; Dang, L.; McNeill, C. R.; Caironi, M.; Noh, Y. Y.; Kim, Y. H. *Adv. Funct. Mater.* **2016**, *26*, 4984.
(35) Cho, J.; Yu, S. H.; Chung, D. S. *J. Mater. Chem. C* **2017**, *5*, 2745.
(36) Chang, C. C.; Chen, C. P.; Chou, H. H.; Liao, C. Y.; Chan, S. H.; Cheng, C. H. *J. Polym. Sci., Part A: Polym. Chem.* **2013**, *51*, 4550.
(37) Chang, H. H.; Tsai, C. E.; Lai, Y. Y.; Liang, W. W.; Hsu, S. L.; Hsu, C. S.; Cheng, Y. J. *Macromolecules* **2013**, *46*, 7715.
(38) Yao, K.; Intemann, J. J.; Yip, H.-L.; Liang, P.-W.; Chang, C.-Y.; Zang, Y.; Li, Z.; Chen, Y.; Jen, A. K.-Y. *J. Mater. Chem. C* **2014**, *2*, 416.
(39) Sulas, D. B.; Yao, K.; Intemann, J. J.; Williams, S. T.; Li, C. Z.; Chueh, C. C.; Richards, J. J.; Xi, Y.; Pozzo, L. D.; Schlenker, C. W.; Jen, A. K.-Y.; Ginger, D. S. *Chem. Mater.* **2015**, *27*, 6583.
(40) Li, Y.; Zhong, L.; Wu, F.-P.; Yuan, Y.; Bin, H.; Jiang, Z.-Q.; Zhang, Z.; Zhang, Z.-G.; Li, Y.; Liao, L. *Energy Environ. Sci.* **2016**, *9*, 3429.
(41) Mcculloch, B. I.; Salleo, A.; Chabinyc, M. *Science* **2016**, *352*, 1521.
(42) Bittle, E. G.; Basham, J. I.; Jackson, T. N.; Jurchescu, O. D.; Gundlach, D. J. *Nat. Commun.* **2016**, *7*, 10908.
(43) Getmanenko, Y. A.; Tongwa, P.; Timofeeva, T. V.; Marder, S. R. *Org. Lett.* **2010**, *12*, 2136.
(44) Xu, S.; Shangguan, X.; Li, H.; Zhang, Y.; Wang, J. *J. Org. Chem.* **2015**, *80*, 7779.
(45) Earmme, T.; Hwang, Y.; Murari, N. M.; Subramaniyan, S.; Jenekhe, S. A. *J. Am. Chem. Soc.* **2013**, *135*, 14960.
(46) Modjewski, M.; Lindeman, S. V.; Rathore, R. *Org. Lett.* **2009**, *11*, 4656.
(47) Sze, S. M.; Ng, K. K. *Physics of Semiconductor Devices*, 3rd ed.; John Wiley & Sons: New York, 2007; p 216.
(48) Lin, Y. H.; Faber, H.; Rossbauer, S.; Anthopoulos, T. D. *Appl. Phys. Lett.* **2013**, *102*, 193516.
(49) Kirby, N. M.; Mudie, S. T.; Hawley, A. M.; Cookson, D. J.; Mertens, H. D. T.; Cowieson, N.; Samardzic-Boban, V. *J. Appl. Crystallogr.* **2013**, *46*, 1670.
(50) Ilavsky, J. *J. Appl. Crystallogr.* **2012**, *45*, 324.
(51) Zhao, C.; Zhang, Y.; Ng, M. K. *J. Org. Chem.* **2007**, *72*, 6364.
(52) Zhong, H.; Han, Y.; Shaw, J.; Anthopoulos, T. D.; Heeney, M. *Macromolecules* **2015**, *48*, 5605.
(53) Pal, B.; Yen, W.; Yang, J.; Chao, C.; Hung, Y.; Lin, S.; Chuang, C.; Chen, C.; Su, W. *Macromolecules* **2008**, *41*, 6664.
(54) Zhang, W.; Smith, J.; Watkins, S.; Gysel, R.; Mcgehee, M.; Salleo, A.; Kirkpatrick, J.; Ashraf, S.; Anthopoulos, T. D.; Heeney, M.; McCulloch, I. *J. Am. Chem. Soc.* **2010**, *132*, 11437.
(55) Endo, K.; Ohkubo, T.; Hirokami, M.; Shibata, T. *J. Am. Chem. Soc.* **2010**, *132*, 11033.
(56) Lee, J. C. H.; McDonald, R.; Hall, D. G. *Nat. Chem.* **2011**, *3*, 894.
(57) Li, H.; Zhang, Z.; Shangguan, X.; Huang, S.; Chen, J.; Zhang, Y.; Wang, J. *Angew. Chem., Int. Ed.* **2014**, *53*, 11921.
(58) Endo, K.; Ishioka, T.; Shibata, T. *Synlett* **2014**, *25*, 2184.
(59) Venkateshvaran, D.; Nikolka, M.; Sadhanala, A.; Lemaur, V.; Zelazny, M.; Kepa, M.; Hurhangee, M.; Kronemeijer, A. J.; Pecunia, V.; Nasrallah, I.; Romanov, I.; Broch, K.; Mcculloch, I.; Emin, D.; Olivier, Y.; Cornil, J.; Beljonne, D.; Sirringhaus, H. *Nature* **2014**, *515*, 384.
(60) Deng, Y.; Chen, Y.; Zhang, X.; Tian, H.; Bao, C.; Yan, D.; Geng, Y.; Wang, F. *Macromolecules* **2012**, *45*, 8621.
(61) Marszalek, T.; Li, M.; Pisula, W. *Chem. Commun.* **2016**, *52*, 10938.
(62) Zhang, M.; Tsao, H. N.; Pisula, W.; Yang, C.; Mishra, A. K.; Müllen, K. *J. Am. Chem. Soc.* **2007**, *129*, 3472.
(63) Kang, I.; An, T. K.; Hong, J. a.; Yun, H. J.; Kim, R.; Chung, D. S.; Park, C. E.; Kim, Y. H.; Kwon, S. K. *Adv. Mater.* **2013**, *25*, 524.
(64) Earmme, T.; Hwang, Y. J.; Murari, N. M.; Subramaniyan, S.; Jenekhe, S. A. *J. Am. Chem. Soc.* **2013**, *135*, 14960.
(65) Dou, L.; Chang, W. H.; Gao, J.; Chen, C. C.; You, J.; Yang, Y. *Adv. Mater.* **2013**, *25*, 825.
(66) Uy, R. L.; Yan, L.; Li, W.; You, W. *Macromolecules* **2014**, *47*, 2289.
(67) Hendriks, K. H.; Li, W.; Wienk, M. M.; Janssen, R. A. J. *J. Am. Chem. Soc.* **2014**, *136*, 12130.
(68) Warnan, J.; El Labban, A.; Cabanetos, C.; Hoke, E. T.; Shukla, P. K.; Risko, C.; Brédas, J. L.; McGehee, M. D.; Beaujuge, P. M. *Chem. Mater.* **2014**, *26*, 2299.
(69) Patra, A.; Bendikov, M. *J. Mater. Chem.* **2010**, *20*, 422.
(70) Keshtov, M. L.; Kuklin, S. A.; Radychev, N. A.; Nikolaev, A. Y.; Koukaras, E. N.; Sharma, A.; Sharma, G. D. *RSC Adv.* **2016**, *6*, 14893.
(71) Hai, J.; Shi, G.; Yu, J.; Zhu, E.; Bian, L.; Ma, W.; Tang, W. *New J. Chem.* **2014**, *38*, 4816.
(72) Li, W.; Hendriks, K. H.; Furlan, A.; Zhang, A.; Wienk, M. M.; Janssen, R. A. J. *Chem. Commun.* **2015**, *51*, 4290.
(73) Keshtov, M. L.; Kuklin, S. A.; Radychev, N. A.; Nikolaev, A. Y.; Ostapov, I. E.; Krayushkin, M. M.; Konstantinov, I. O.; Koukaras, E. N.; Sharma, A.; Sharma, G. D. *Phys. Chem. Chem. Phys.* **2016**, *18*, 8389.
(74) Zhou, E.; Cong, J.; Hashimoto, K.; Tajima, K. *Energy Environ. Sci.* **2012**, *5*, 9756.
(75) Jung, J. W.; Liu, F.; Russell, T. P.; Jo, W. H. *Energy Environ. Sci.* **2012**, *5*, 6857.
(76) Tsao, H. N.; Cho, D. M.; Park, I.; Hansen, M. R.; Mavrinskiy, A.; Yoon, D. Y.; Graf, R.; Pisula, W.; Spiess, H. W.; Müllen, K. *J. Am. Chem. Soc.* **2011**, *133*, 2605.
(77) Wang, S.; Kappl, M.; Liebewirth, I.; Müller, M.; Kirchhoff, K.; Pisula, W.; Müllen, K. *Adv. Mater.* **2012**, *24*, 417.
(78) Yamashita, Y.; Tsurumi, J.; Hinkel, F.; Okada, Y.; Soeda, J.; Zajączkowski, W.; Baumgarten, M.; Pisula, W.; Matsui, H.; Müllen, K.; Takeya, J. *Adv. Mater.* **2014**, *26*, 8169.
(79) Pattanasattayavong, P.; Promarak, V.; Anthopoulos, T. D. *Adv. Electron. Mater.* **2017**, *3*, 1600378.
(80) Wijeyasinghe, N.; Anthopoulos, T. D. *Semicond. Sci. Technol.* **2015**, *30*, 104002.
(81) Niedzialek, D.; Lemaur, V.; Dudenko, D.; Shu, J.; Hansen, M. R.; Andreasen, J. W.; Pisula, W.; Müllen, K.; Cornil, J.; Beljonne, D. *Adv. Mater.* **2013**, *25*, 1939.
(82) Tsao, H. N.; Cho, D.; Andreasen, J. W.; Rouhanipour, A.; Breiby, D. W.; Pisula, W.; Müllen, K. *Adv. Mater.* **2009**, *21*, 209.
(83) Pattanasattayavong, P.; Yaacobi-Gross, N.; Zhao, K.; Ndjawa, G. O. N.; Li, J.; Yan, F.; O'Regan, B. C.; Amassian, A.; Anthopoulos, T. D. *Adv. Mater.* **2013**, *25*, 1504.


DOI: 10.1021/jacs.7b03099
*J. Am. Chem. Soc.* 2017, 139, 8552−8561